Al-Azhar University Civil Engineering Research Magazine (CERM)
Vol. (39) No. (1) January, 2017

HYSTERETIC BEHAVIOR OF STEEL FIBER REINFORCED CONCRETE BRIDGE COLUMNS

Abdel-rahman Mohamed Naguib a, Nayer Ahmed El-Esnawy b, Ahmed Mahmoud Saleh c, Waleed Abdel-latif Atteya c

a Lecturer Assistant, Civil Engineering Department, MTI University, Cairo, Egypt, and PhD candidate, Dept. of Structural Engineering, Cairo University, Giza, Egypt
b Professor, Dept. of Structural Engineering, Cairo University, Giza, Egypt (on leave as Head of Civil Engineering Department, Faculty of Engineering and Technology, Badr University in Cairo, Egypt)
c Professor, Dept. of Structural Engineering, Cairo University, Giza, Egypt

ملخص:

اكتسبت الخرسانة المسلحة بالألياف اهتمام المهندسين الإنشائيين فى العقود القليلة الماضية. و بالرغم من وجود العديد من المواصفات الأمريكية و الأوروبية، يوجد معلومات قليلة عن سلوك الخرسانة المسلحة بالألياف باالكود المصري للتصميم. وبالتالي يهدف هذا البحث إلي استعراض الخصائص الميكانيكية، مثل مقاومة الضغط المحورى ، مقاومة الشد المحورى ، و معاير الكسر، بدراسة عينات قياسية تحتوى على نسب مختلفة من الالياف الحديدية ٠,٥% ، ١% ، ١,٢٥% ، ٢% بالحجم ومقارنتها بالخصائص الميكانيكية لعينات من الخرسانة العادية. كذلك يهدف هذا البحث إلي دراسة مدى كفاءة استخدام الخرسانة المسلحة بالألياف الحديدية فى أعمدة الكبارى الخرسانية لمقاومة أحمال الزلازل، وذلك باختبار السلوك الزلزالى لثمانية نماذج مصغرة بنسبة ١:٤ لأعمدة الكبارى تحت تأثير حمل جانبي ترددى بمعدل بطيء في وجود قوة محورية ضاغطة علي العمود بقيمة ثابتة. وتم دراسة تأثير المتغيرات التالية: نسبة الحديد الطولى و العرضى و محتوى الألياف الحديدية، وعمل مقارنة مع السلوك الزلزالى لعينة من الخرسانة المسلحة بدون الالياف الحديدية. و قد أظهرت النتائج التحسن الناتج عن استخدام الألياف الحديدية فى أعمدة الكبارى من حيث الممطولية و القدرة على أمتصاص الطاقة و تماسك العنصر الخرساني و توزيع الشروخ.

ABSTRACT

Steel fiber reinforced concrete (SFRC) has gained extensive attention as a construction material for structural applications in the last few decades. Unlike several international codes, there is little information about the behavior of SFRC as a construction material in the Egyptian code of practice. So, this study has two objectives. Firstly, the mechanical properties of the SFRC material are demonstrated: the axial compressive strength, the axial tensile strength, and the modulus of rapture. This is achieved by examining several specimens with different steel fiber content of 0.5%, 1.0%, 1.5%, and 2.0% by volume in compression and comparing their mechanical properties with those of plain concrete. Secondly, the efficiency of using SFRC in the construction of bridge columns to resist earthquakes is studied. This is achieved by investigating the hysteretic behavior of eight quarter-scaled bridge columns via quasi-static tests of repeated lateral loading and unloading of the scaled bridge columns when subjected to a dead axial compressive force. The parameters considered are the steel fiber content, as well as the longitudinal and lateral reinforcement ratios. The hysteresis loops of SFRC bridge columns are developed and compared with those of reinforced concrete columns. The experimental results show that using the SFRC material in construction of bridge columns provides higher ductility, larger capacity for energy absorption, better integrity of concrete, and lesser crack distribution.

Keywords: Steel fibers; SFRC; Mechanical properties; Hysteretic behavior; Bridge columns; Ductility; Earthquake response; Quasi-static tests; Crack distribution.

INTRODUCTION

The low tensile strength of plain concrete (PC) and its brittle failure nature require using steel bars as a reinforcing material in zones of tensile stresses. However, under cycles of repeated loading and unloading due to an earthquake event, concrete crushes into small parts and looses its integrity or debones from its reinforcing steel bars. Also, buckling of longitudinal rebars and opening of transversal ties can occur, and thus the concrete member fails. Many tests were made to increase the tensile strength and integrity of the plain concrete. Among them, discrete steel fibers have been added to the ingredients of concrete during the mixing process. These steel fibers act as links between cracks, and, therefore, the tensile strength is increased and the concrete integrity is retained. The concept of crack bridging through discrete steel fibers is introduced in ACI 544.1R-96, ACI 544.2R-89, ACI 544.3R-93, ACI 544.4R-88, ACI 544.5R-10 [1-5], and EN 14889-1:2006 [6]. The properties of steel fibers and the manufacturing details are listed in ASTM A820 / A820M – 11[7]. Unfortunately, there is little information in the Egyptian code of practice about steel fiber reinforced concrete (SFRC) material. Thus, several researchers in Egypt have explored this concept of using SFRC in the construction industry. Some researchers studied the mechanical properties of steel fiber reinforced concrete [8]. Others studied the effect of using SFRC in beams [9-12], beam-column joints [13], flat slabs [14], and post tension concrete beams [15]. Their results showed the benefit of using SFRC in different concrete applications on the basis of strength and energy absorption capacity.

Abroad, Kumar et. al. [16] investigated the effect of using SFRC in bridge columns for resisting earthquakes. Two 1:4.5 scale circular columns subjected to uni-directional cyclic loadings in the presence of constant axial load were tested and compared to a typical reinforced concrete column with the same dimensions and reinforcement. More ductile behavior in both tension and compression was observed compared to the typical RC column. Also, SFRC scaled columns were able to resist spalling of the concrete cover up to a drift ratio of 3.6%, which was more than the typical RC column.

The objective of this study is two-fold. Firstly, the effect of adding discrete steel fibers with different dosages to the concrete mix on the mechanical properties of concrete is studied. Secondly, the efficiency of using SFRC in bridge columns for resisting earthquakes is investigated. The first objective is achieved by testing 15 concrete standard cubes, 15 concrete standard cylinders, and 15 concrete standard prisms in axial compression test, indirect tension test, and three-point bending test. The second objective is achieved by testing 8 quarter-scaled bridge columns with different steel fiber dosages under uni-directional cycles of loading and unloading applied in a quasi-static manner and in the presence of a dead axial compression force.

EXPERIMENTAL PROGRAM

The experimental program consists of two phases. The first phase focuses on studying the influence of adding steel fibers on the mechanical properties of concrete. Four fiber dosages of 0.5%, 1.0%, 1.5%, and 2.0% by volume are added to the concrete mix. Total of 45 specimens have been tested: 15 standard cubes (150x150x150 mm), 15 cylinders (150x300 mm), and 15 prisms (150x150x600 mm). The second phase focuses on

investigating the effect of adding steel fibers on the hysteretic behavior of reinforced concrete bridge columns. Eight quarter-scaled bridge columns (300x400x2100 mm) with shear span of 1800 mm have been tested. The dimensions were selected such that shear span to depth ratio is 6.0, which ensures flexure dominated failure mode. A dead axial compression force of 15% the nominal load (equal to 588 KN) has been applied to all scaled columns via a hydraulic jack. The control column with no steel fiber content is denoted by S1. In the meantime, S2, S3, S4, and S5 include steel fiber dosages of 0.75%, 1.0%, 1.25%, and 1.5% by volume, respectively. In column specimen S6, and different from all other columns, no doubling of stirrups at plastic hinge zone exists. In column specimen S7, steel fiber dosage of 1% is used and the longitudinal steel bars ratio decreased to be 2.12%, instead of the 2.54% used in all the other column specimens. In column specimen S8, the steel fiber dosage is 1% placed only at the lower third of column height and no steel fibers in the remaining height. All specimens have lap splices at mid height. Figure 1 shows main details of all tested scaled columns.

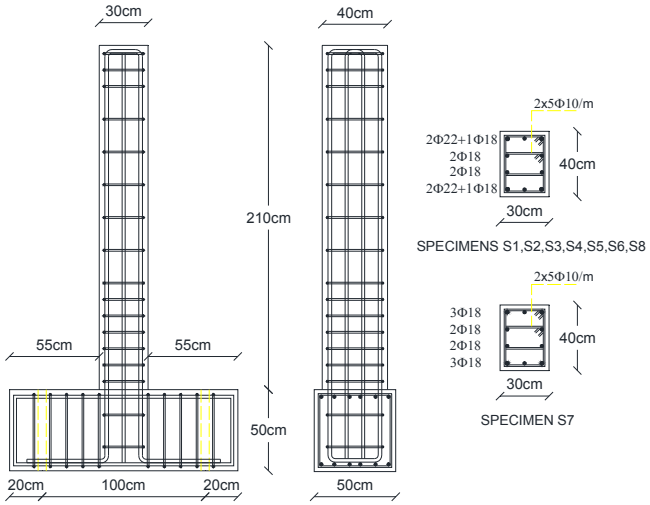

Fig. 1: Details of tested scaled bridge columns

2.1 Material Properties

Concrete ingredients was brought from the Arab contractors company; a leading construction company in Egypt to simulate the concrete used in the local market. They provided ordinary Portland cement CEM I 42.5 from TORA factory, while natural sand was from EL-LEWAA district, for crushed limestone (Dolomite) was from ATAQA district. Super plasticizer was SIKAMENT R2004 from SIKA Company, while pure drinking water is used for mixing. Table 1 shows the quantities required for one cubic meter of fresh concrete to achieve the target concrete cubic compressive strength of 40 MPA. High strength deformed bars grade 40/60 brought also from Arab contractors company workshop at 10th of Ramadan city with diameters 22mm, 18mm for longitudinal main steel and 10mm for the lateral reinforcement. Steel fibers had corrugated shape with 50 mm in length and rounded cross section of 1.0 mm in diameter, with length to diameter ratio of 50. Fibers brought from the world company for drawing and manufacturing wires at KANATER ALKHAIREYA district. Three cubes and three

cylinders were prepared during casting of each specimen for quality assurance purposes and cured the same way for curing specimens, and then tested on the same testing day for each specimen.

Table 1: Proportions of concrete mixes for 1m3

	Cement (Kg)	Dolomite (Kg)	Sand (Kg)	Water (Liter)	Plasticizer (Liter)	Steel Fiber Volume (%)
First Part	400	1040	680	190	3	0.5 - 1.0 1.5 - 2.0
Second Part	450	1060	670	190	7	0.75 - 1.0 1.25 -1.50

2.2 Test Setup

For the first phase where the influence of adding steel fibers on mechanical properties of concrete is studied, Fig. 2.a illustrates the steel fiber type, Fig. 2.d illustrates the standard uniaxial compression test for cubes to determine the axial compressive strength. While Fig. 2.e and Fig. 2.f illustrates the indirect tension test to determine the splitting tension strength. For determining the modulus of rapture, Fig. 2.g and Fig. 2.h illustrates the three point bending test.

For the second phase to study the efficiency of using SFRC in bridge columns for resisting earthquakes, the hysteretic behavior was examined through Quasi-static tests of repeated lateral load in the presence of constant axial compressive load. These tests were performed in the reinforced concrete laboratory of the housing and building research center (HBRC) at Giza, Egypt. Fig. 4 illustrates the test setup. Two lateral LVDTs (Linear Voltage Displacement Transducers) located at 0.90m and 1.80 from footing top were attached to the specimen. In addition, two vertical LVDTs were attached on the column both sides to be used in curvature calculations. Each column specimen had eight strain gages, four on the longitudinal reinforcement with gage length of 10mm, and two strain gages on the lateral reinforcement with gage length of 6mm. In addition two strain gages stacked on concrete surface to measure longitudinal and lateral strain of concrete with gage length of 60 mm.

2.3 Testing Procedure

For the first phase, all tests were performed according to ECP-203 [17]. After placing specimens, the compressive force was applied through a hydraulic jack in a static manner, then the maximum load was determined. Compressive strength, indirect tension strength, and modulus of rapture were calculated according to ECP-203. For the second phase, an axial compression force of 588 KN was applied through a hydraulic jack on the top of column, then the lateral jack was attached and its screws were fastened. Then, the screws of the vertical LVDTs were fastened and all wires of the LVDTs and strain gages were connected to the data acquisition system. Next step is to reset all readings in the data acquisition system, and then start to apply the displacement protocol as illustrated in Fig. 3. Displacement scenario was selected based on ATC-24 protocol [18]. The system automatically saves the measured displacement, the measured lateral load and all recorded data from the strain gages, LVDTs, and axial load cell.

Fig. 2: Specimens preparation and testing, a) Steel fiber, b) During casting ,c) Samples after curing, d)Cubes during testing , e) Cylinder preparation for testing, f) Cylinder during testing, g) Prism preparation for testing, h) Prism during testing

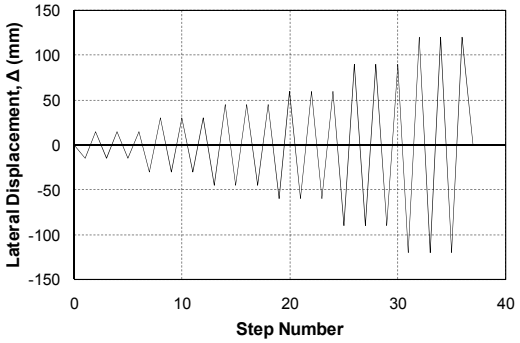

Fig. 3: Loading scenario of tests

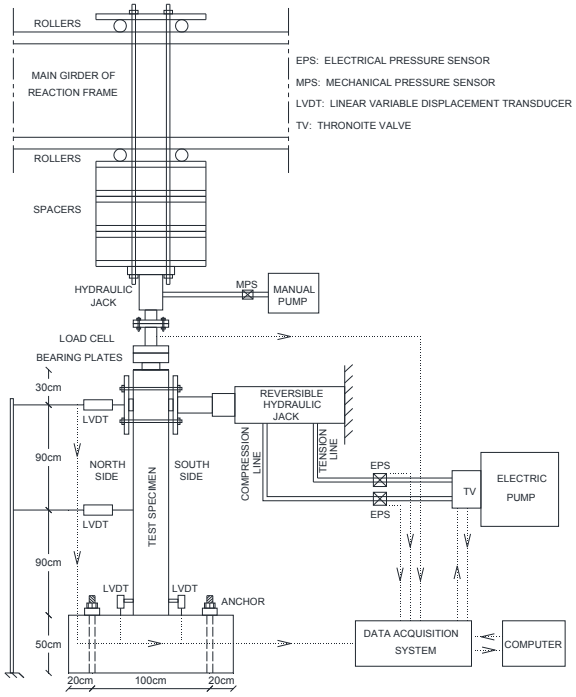

Fig. 4: Schematic of test setup

EXPERIMENTAL RESULTS, ANALYSIS AND DISCUSSION

3.1 Modes of Failure

For the first phase, Fig. 5 illustrates that the plain concrete specimens crushed, or divided into two pieces, while the SFRC ones reserved their integrity. Also, table 2 illustrates that there was an increase in the compressive strength ranged from 13% up to 27%. Regarding tensile strength, there was an increase of 14.1% up to 44.2%. Modulus of rapture also had an increase from 15.2% up to 53.2%.

For the second phase, and as all specimens were selected such that the shear span to depth ratio equal to 6, all specimens were failed in bending by developing plastic hinge at column bottom. Cracks developed in the first few cycles and its number kept constant throughout the test, but of course its width increased. As expected, the specimen S1 experienced the maximum damage at plastic hinge zone, spalling of concrete cover can

be noticed from Fig. 10.e. All other specimens had lower damage at plastic hinge than specimen S1, it can be noticed from Fig. 11.e to Fig. 17.e.

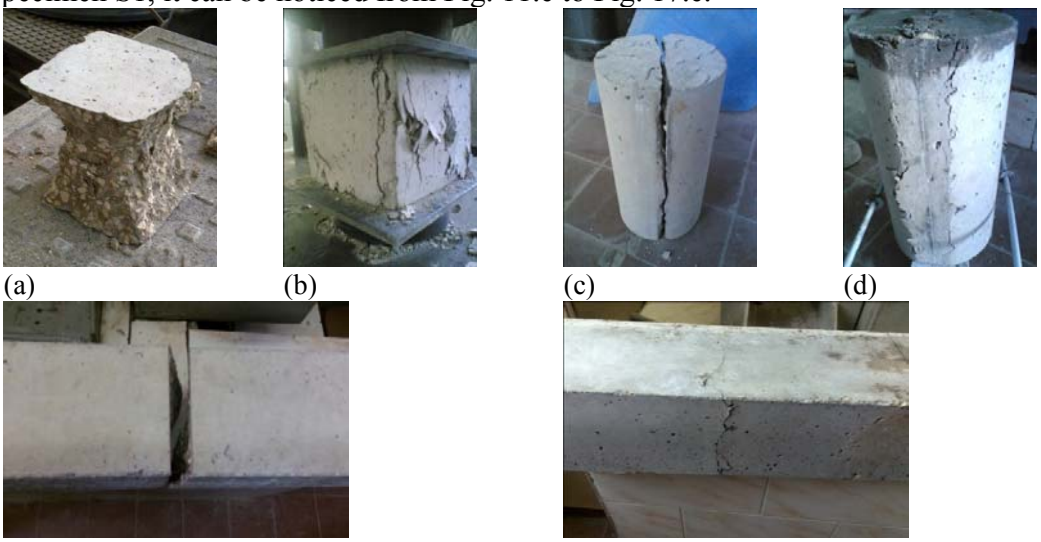

(a) (b) (c) (d)

(e) (f)

Fig. 5: Mode of failure for specimens, a) PC cube after testing, b) SFRC cube after testing , c) PC cylinder after testing, d) SFRC cylinder after testing, e) PC prism after testing, f) SFRC prism after testing.

3.2 Load–Displacement Relationships and Strength Evaluation

The load-displacement hysteresis loops are illustrated from Fig. 10.b to Fig. 17.b and the strength envelopes of the different specimens are presented in Fig. 6. Also, Table 3 shows the comparison between the loads needs to reach 7.5 mm in the first, the yield displacement, the ultimate load and its corresponding lateral displacement.

Table 2: Results of the 45 specimens concerning the first phase

	Fiber dose (%)	control	0.5	1	1.5	2
Cubes	Ultimate Load (KN)	786.7	906.9	951.6	990.1	1020
		796	899.2	960.6	987.2	1018.7
		807.4	894.6	957.9	997.8	1011.3
	Average	796.7	900.2	956.7	991.7	1016.7
	Stress (Mpa)	35.4	40.0	42.5	44.1	45.2
	Enhancement (%)	0.0	13.0	20.1	24.5	27.6
Cylinders	Ultimate Load (KN)	243.3	263.5	303.8	334.9	351
		232.4	277.8	301.5	337.8	331.5
		248.8	285.2	303.5	335.3	362.5
	Average	241.5	275.5	302.9	336.0	348.3
	Stress (Mpa)	3.4	3.9	4.3	4.8	4.9
	Enhancement (%)	0.0	14.1	25.4	39.1	44.2
Prisms	Ultimate Load (KN)	26.5	32.5	37	41.5	42.5
		30.5	31.5	37.5	39.5	43.5
		28.5	34.5	35.5	38.5	45
	Average	28.5	32.8	36.7	39.8	43.7
	Stress (Mpa)	5.7	6.6	7.3	8.0	8.7
	Enhancement (%)	0.0	15.2	28.7	39.8	53.2

Table 3: The experimental results of tested specimens concerning the second phase

SPECIMEN	P1 (first cycle load at 7.5 mm displacement) (KN)	Pu (Ultimate load) (KN)	Δu (displacement at Pu (mm)	Δf (displacement at failure) (mm)	Δy (Yeild displacement) (mm)
S1	52.70	164.65	75.78	>91.03	25.34
S2	58.35	141.88	65.44	>122.28	21.03
S3	55.66	124.49	45.04	>122.08	23.43
S4	53.87	138.75	73.85	>121.14	21.20
S5	54.05	156.71	60.33	>122.89	29.85
S6	53.24	151.11	60.031	>121.89	27.67
S7	58.49	126.11	28.51	>90.44	20.08
S8	53.81	183.77	45.91	>126.21	32.60

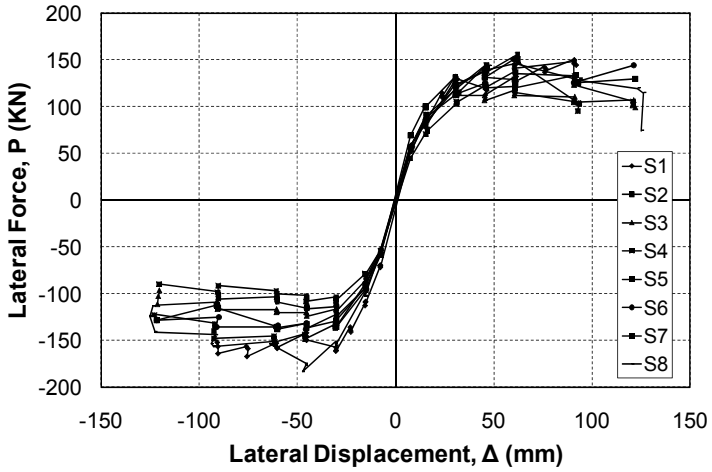

Fig. 6: Load-displacement hysteresis envelope of the tested specimens

3.3 Yield, Failure Displacement, Displacement Ductility Factor and Accumulated Displacement Ductility

The yield displacement for an equivalent elastic-plastic system with reduced cracked stiffness was calculated from the lateral load-displacement curve as the corresponding displacement of intersection of the secant stiffness (at either the first yield or at a load value of 75% of the ultimate lateral load whichever is less) and a tangent stiffness at the ultimate load. The first yield could not be accurately determined during the test program; hence the evaluation of yield displacement is based on the value of 75% of ultimate lateral load as shown in Fig. 7.

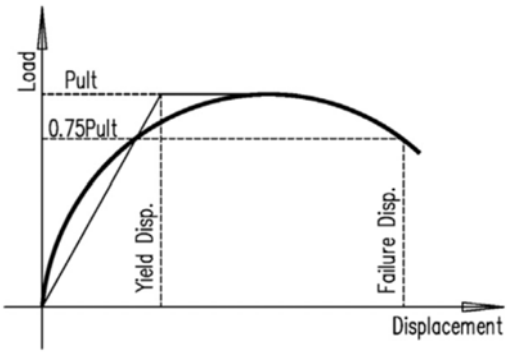

Fig. 7: Determination of yield and failure displacement.

The displacement ductility is defined as the ratio between the maximum displacement at cyclic number i, Δi, and the yield displacement Δy.

Displacement ductility = Δi / Δy (1)

Also, the displacement ductility factor is defined as the ratio between the displacement at failure, Δf, and the yield displacement Δy.

Displacement ductility factor = Δf / Δy (2)

The accumulated displacement ductility is defined as the sum of the displacement ductility up to the defined failure load.

Accumulated displacement ductility =Σ (Δi / Δy) (3)

where Δi is the maximum displacement at cycle number i. Table 4 shows the displacement ductility factors and the accumulated displacement ductility for the test specimens.

Table 4: Displacement ductility factor

SPECIMEN	Displacement ductility factor	Accumulated Ductility up to 5% top drift ratio
S1	>3.59	28.75
S2	>5.81	34.51
S3	>5.21	30.95
S4	>5.71	34.32
S5	>4.12	24.77
S6	>4.41	26.33
S7	>4.50	36.08
S8	>3.87	22.84

3.4 Energy Dissipation Characteristics

The capability of a structure to withstand an earthquake depends on its ability to dissipate the energy input from ground motion. Despite the fact that energy input during a earthquake is difficult to estimate, a satisfactory design should ensure a larger energy dissipation capability of the structure than the demand. Fig. 8 illustrates the variation of the cumulative dissipated energy with the lateral displacement for all specimens. The dissipated energy was computed for each cycle as the area enclosed by the lateral load–displacement hysteresis loop for the cycle. The area was computed using Eq. (4).

Ei =[(Pi+1 + Pi) * (Δi+1 - Δi) / 2] (4)

Where Ei energy dissipated per cycle, Pi and Pi+1 are the lateral loads at intervals number i, and i+ 1, Δi and Δi+1 are the lateral displacement at intervals number i, and i+ 1.

A non dimensional energy index is used to evaluate the energy dissipated by different test specimens. In the current study, the normalized energy index (IEN), proposed by Ehsani and Wight [19] was used as a reliable and comprehensive measure of dissipated energy. It has the advantage of including the effect of actual displacement, stiffness and energy for each cycle. Consequently, this index is sensitive in evaluating any variations in the seismic performance of beam-column joints. The normalized energy index, IEN, is expressed as follows:

$$I_{EN} = \frac{1}{P_y \Delta_y} \sum_{i=1}^{m} E_i \left(\frac{K_i}{K_y} \right) \left(\frac{\Delta_i}{\Delta_y} \right)^2 \quad (5)$$

Where Ei is the energy dissipated during ith cycle of loading, Δy is the yield displacement of the specimen, Py is the yield load, Ky is the stiffness corresponding to the yield displacement and, Δi is the peak displacement of the ith cycle and Ki is the corresponding stiffness. The specimen having a normalized energy dissipation index of 60 or higher possesses sufficient ductility to satisfy the requirements of Committee 352 recommendations [20]. Table 5 summarizes these results.

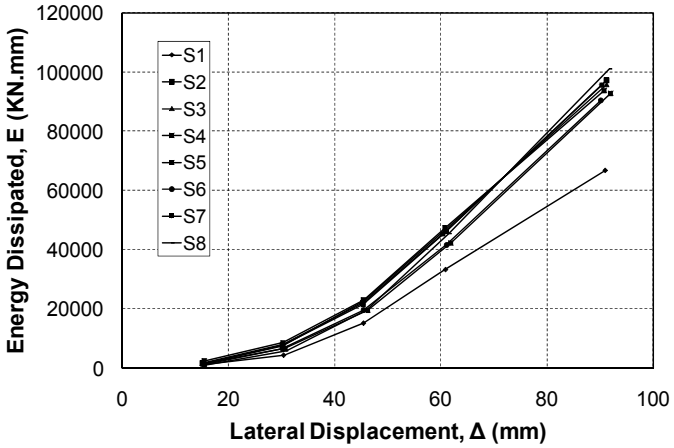

Fig. 8: Energy dissipation of the tested specimens

Table 5: Total accumulated energy and the energy index of the specimens

SPECIMEN	Total accumulated energy up to test end (KN. mm)	Total accumulated energy up to 5% top drift ratio (KN. mm)	IEN (up to 5% top drift ratio)
S1	66742.51	66742.51	54.41
S2	126186.90	97235.53	129.97
S3	164982.92	95753.03	112.29
S4	140240	93741.18	140.80
S5	113820.30	92755.63	55.87
S6	117659.40	90354.81	68.19
S7	95568.82	95568.82	128.32
S8	187083.84	100907.88	41.16

3.5 Stiffness Analysis

The cracked stiffness of each of the specimens was calculated for every loading cycle. The cracked stiffness was computed as follows:

$$K_i = P_i / \Delta_i \quad (6)$$

where: P_i is the maximum load at cycle i , and Δ_i is the maximum displacement at cycle i. The cracked stiffness versus the lateral displacement to represent the stiffness degradation due to cyclic loading of the tested eight specimens is illustrated in Fig. 9 and table 6.

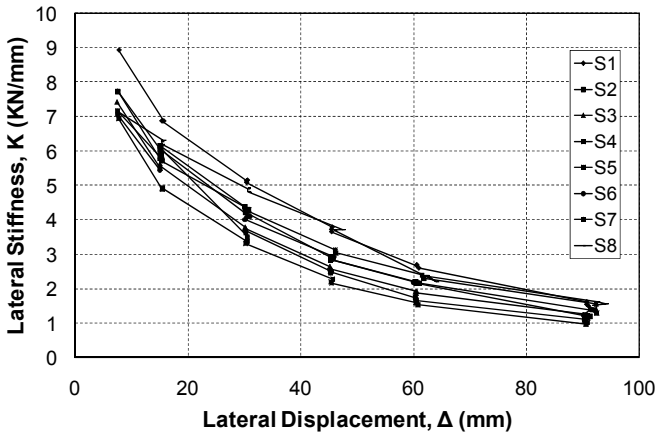

Fig. 9: Stiffness degradation of the tested specimens.

Table 6: Lateral Stiffness at different lateral displacement levels

SPECIMEN	Lateral Stiffness, K (KN/mm)					
	7.5mm	15mm	30mm	45mm	60mm	90mm
S1	8.92	6.87	5.09	3.66	2.60	1.50
S2	7.73	6.15	4.21	2.85	2.15	1.18
S3	7.42	5.56	3.74	2.55	1.86	1.14
S4	6.94	4.91	3.31	2.16	1.53	1.02
S5	7.17	5.70	4.24	3.03	2.29	1.39
S6	7.07	6.04	4.01	2.85	2.17	1.23
S7	7.74	6.07	3.69	2.48	1.66	1.06
S8	7.16	6.19	4.80	3.69	2.39	1.52

(a)

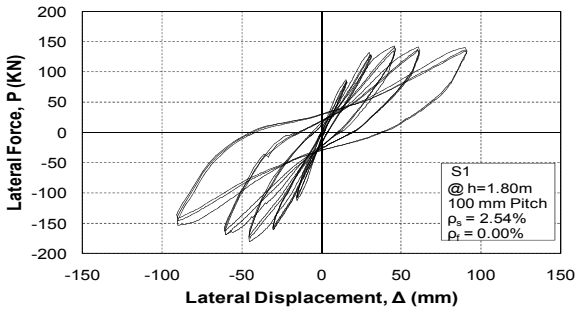

(b)

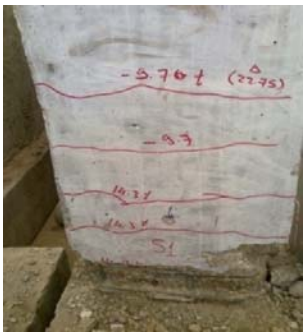

(c)

(d)

(e)

(f)

Fig. 10: Specimen S1, a) During testing, b) Hysteresis loops , c) Crack distribution at north side, d) Crack distribution at south side, e) Damage at north side, f) Damage at south side

(a)

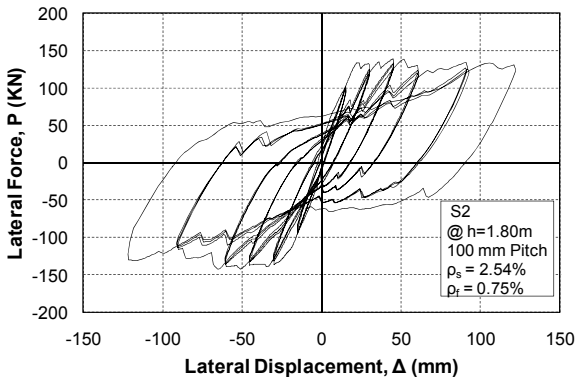

(b)

(c)

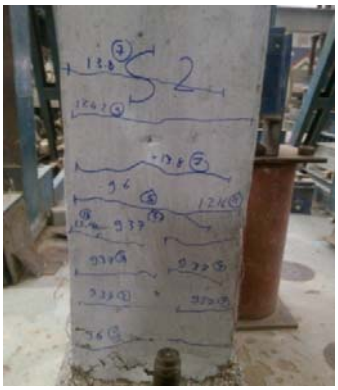

(d)

(e)

(f)

Fig. 11: Specimen S2, a) During testing, b) Hysteresis loops , c) Crack distribution at north side, d) Crack distribution at south side, e) Damage at north side, f) Damage at south side

(a)

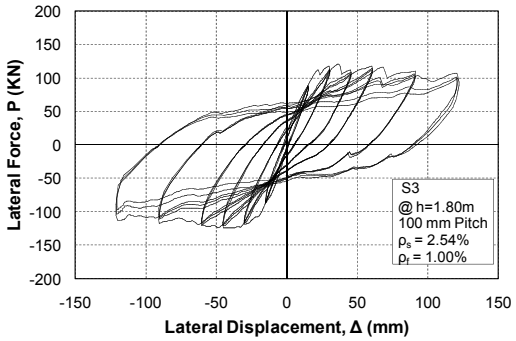

(b)

(c)

(d)

(e)

(f)

Fig. 12: Specimen S3, a) During testing, b) Hysteresis loops , c) Crack distribution at north side, d) Crack distribution at south side, e) Damage at north side, f) Damage at south side

(a)

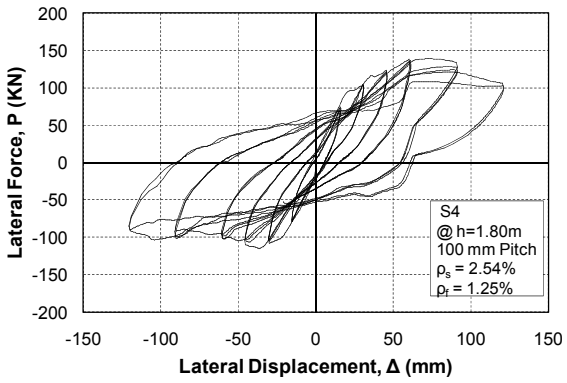

(b)

(c)

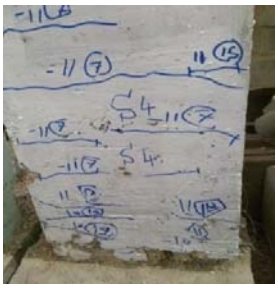

(d)

(e)

(f)

Fig. 13: Specimen S4, a) During testing, b) Hysteresis loops , c) Crack distribution at north side, d) Crack distribution at south side, e) Damage at north side, f) Damage at south side

(a)

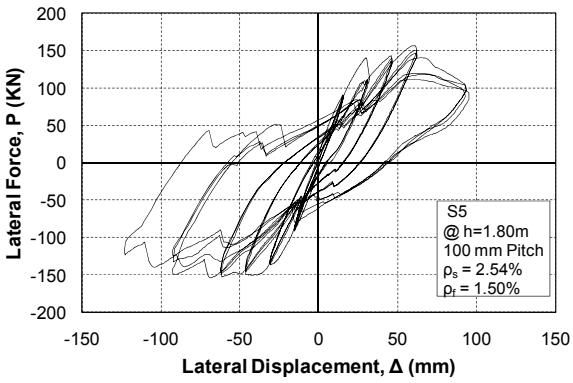

(b)

(c)

(d)

(e)

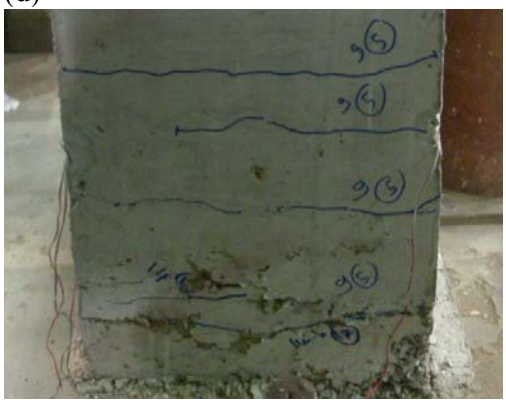

(f)

Fig. 14: Specimen S5, a) During testing, b) Hysteresis loops , c) Crack distribution at north side, d) Crack distribution at south side, e) Damage at north side, f) Damage at south side

(a)

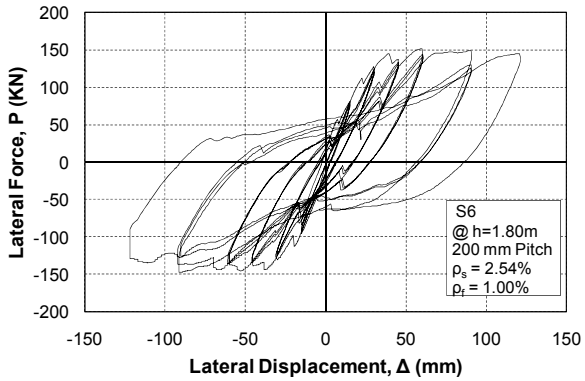

(b)

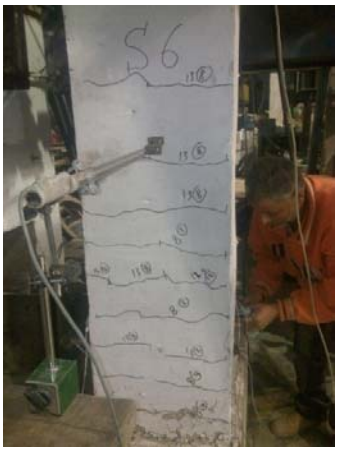

(c)

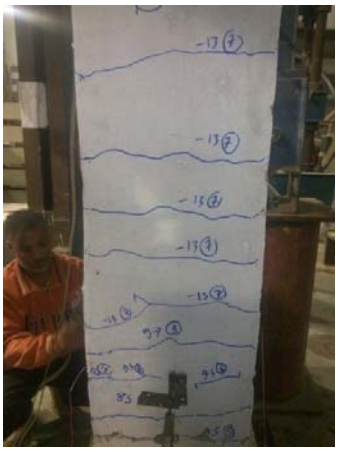

(d)

(e)

(f)

Fig. 15: Specimen S6, a) During testing, b) Hysteresis loops , c) Crack distribution at north side, d) Crack distribution at south side, e) Damage at north side, f) Damage at south side

(a)

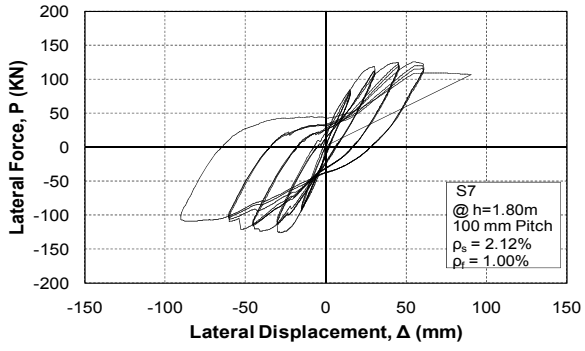

(b)

(c)

(d)

(e)

(f)

Fig. 16: Specimen S7, a) During testing, b) Hysteresis loops , c) Crack distribution at north side, d) Crack distribution at south side, e) Damage at north side, f) Damage at south side

(a)

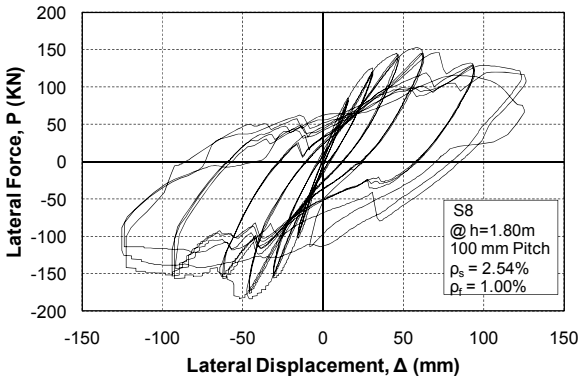

(b)

(c)

(d)

(e)

(f)

Fig. 17: Specimen S8, a) During testing, b) Hysteresis loops , c) Crack distribution at north side, d) Crack distribution at south side, e) Damage at north side, f) Damage at south side

4. CONCLUSIONS

The tensile strength and the integrity of concrete are enhanced by using discrete steel fibers in the concrete mix, since they provided discrete links between cracks. Also, the ductile behavior in tension and compression under cycles of loading and unloading has been achieved using the steel fibers. Energy absorption capacity is increased with the increase of steel fibers content.

For typical RC bridge column S1, cracks appeared at the lower third during the first few cycles of repeated loading, then all damage concentrated in a zone of 15 cm over the column foundation. For the steel fiber reinforced concrete (SFRC) scaled columns (S2 to S7), cracks appeared at the lower half during the first few cycles, then a separation crack at the interface between the column and foundation absorb all deformations via opening and closing mechanism with the aid of reinforcing steel bars that link the crack sides. The major separation crack is formed due to the effect of the random discrete links represented by the steel fibers to retain the integrity of concrete at the plastic hinge zone, which left this zone in a good state. Therefore, one way to permit more deformation is to place this zone further away from the foundation. Behavior of tested column S8, which

had SFRC in the lower third only, was between the behavior of column S1 and the behavior of all other tested columns, where cracks extended to the lower third and the plastic hinge zone had some damage.

The increase in the compressive strength ranges from 13% up to 27%. Regarding the tensile strength, there is an increase of 14% up to 44%. The modulus of rapture has also increased from 15% up to 53%. The range of yield displacement is from 20.1 mm for column S7 to 32.6 mm for column S8, compared to 25.3 mm for typical RC column S1. Accumulated ductility up to 5% top drift ratio ranges from 22.84 for column S8 up to 36.08 for column S7, compared to 28.75 for column S1. Finally, the energy index up to 5% top drift ratio ranges from 41.16 for column S8 up to 140.80 for column S4, compared to 54.41 for column S1.

REFERENCES

[1] American Concrete Institute (ACI) Committee 544, "Report on Fiber Reinforced Concrete", ACI544.1R-96: (Reapproved 2009), Farmington Hills, USA , 1996.

[2] American Concrete Institute (ACI) Committee 544, "Measurement of Properties of Fiber Reinforced Concrete", ACI 544.2R-89: (Reapproved 2009), Farmington Hills, USA, 1989.

[3] American Concrete Institute (ACI) Committee 544, "Guide for Specifying, Proportioning, and Production of Fiber-Reinforced Concrete", ACI 544.3R-08, Farmington Hills, USA, 2008.

[4] American Concrete Institute (ACI) Committee 544, "Design Considerations for Steel Fiber Reinforced Concrete, ACI 544.4R-88 :(Reapproved 2009), Farmington Hills, USA, 1988.

[5] American Concrete Institute (ACI) Committee 544, "Report on the Physical Properties and Durability of Fiber-Reinforced Concrete", ACI 544.5R-10, Farmington Hills, USA, 2010.

[6] European Committee for Standardization (CEN/TC 104), "Fibres for concrete", EN 14889-1:2006, United Kingdom, 2006.

[7] American Society for Testing and Materials, (ASTM) Committee A01.05, "Standard Specification for Steel Fibers for Fiber-Reinforced Concrete", ASTM A820 / A820M - 11, ASTM International, West Conshohocken, PA, USA , 2011.

[8] Wafa FF, and Ashour SA., "Mechanical properties of high strength of fiber reinforced concrete", ACI Material Journal; 89(5):449-455, 1992.

[9] Ahmed S E, and Khaled S R., "Behavior of steel fiber reinforced high strength self-compacting concrete beams under combined bending and torsion", International Journal of Civil and Structural Engineering; 4(3), 2014.

[10] Shereen E T., "Enhancing the behavior of reinforced concrete beams by adding fibers in the mix", M.Sc Thesis: Faculty of Engineering, Helwan University, Cairo, Egypt, 2013.

[11] Ahmed Y., " Shear behavior of high strength R.C. beams with fibers added to concrete mix", M.Sc Thesis: Faculty of Engineering, Helwan University, Cairo, Egypt, 2014.

[12] Nasr Z H, Hala M I, and Amany M S, "Finite element analysis of reinforced concrete beams with fibers added to the mix", 2nd International Conference on Bridge Testing, Monitoring & Assessment; GEN40:1-12, 2015.

[13] Tarek M B., "Seismic behavior of reinforced high-strength concrete beam-column joints with and without steel fibers", PhD Thesis: Faculty of Engineering, Cairo University, Giza, Egypt, 2002.

[14] Essam S K, and Sherif H A., "Improvement of two-way shear behavior for flat slabs using different concrete composites and multi-layer wraps", 2nd International Conference on Bridge Testing, Monitoring & Assessment GEN63:1-25, 2015.

[15] Hossam-eldin A E, Tamer E A, Abdel Wahab E G , and Amr A A. ,"Behavior of post-tensioned fiber concrete beams", HBRC Journal; 9:216-226, 2013.
[16] Kumar, P., Jen, G., Trono, W., Panagiotou, M., and Ostertag, C., "Self Compacting Hybrid Fiber Reinforced Concrete Composites for Bridge Columns", Pacific Earthquake Engineering Research Center, Report No. PEER 2011/106, University of California, Berkeley, USA, 2011.
[17] Egyptian Code of Practice (ECP) Committee 203, "Egyptian Code for Design and Construction of Reinforced Concrete Structures", Housing and Building National Research Center, Giza, Egypt , 2007.
[18] Applied Technology Council (ATC), "Guidelines for Cyclic Seismic Testing of Components of Steel Structures", ATC-24, Applied Technology Council, Redwood City, CA, 1992.
[19] M.R. Ehssani, and J.K. Wight, "Confinement steel requirements for connection ductile frames", J. Struct. Eng. 116; 450–465, 1990.
[20] ACI-ASCE Committee 352, "Recommendations for Design of Beam-Column Connections in Monolithic Reinforced Concrete Structures", American Concrete Institute, 2002.